

*Mechanical validation of the three-dimensional intersection geometry  
between the Puente Hills blind-thrust system and the Whittier fault,  
Los Angeles, California*

**W. A. Griffith and M. L. Cooke**  
**The University of Massachusetts, Amherst**  
**Accepted with revisions to the**  
**Bulletin of the Seismological Society of America**

## **1. Abstract**

*The sensitivity of fault interaction to alternative, kinematically plausible intersection geometries of the Puente Hills blind thrust system and the Whittier fault is modeled under geodetically constrained horizontal contraction. Comparisons of modeled slip rates to available geologic rates 1) suggest that the Coyote Hills segment of the Puente Hills system extends to the base of the seismogenic crust and 2) give slight preference for extension of the active Whittier fault to the base of the seismogenic crust rather than limiting active slip to the hanging wall of the Coyote Hills fault. Furthermore, analysis of strain energy density demonstrates that the preferred model has the greatest mechanical efficiency. This correlation of fit to geologic slip rates and mechanical efficiency supports the effectiveness of this method for evaluating among alternative geometries in the absence of geologically constrained slip rates. The methodology implemented in this study may be effectively used in future studies of deformation within fault systems.*

*Model generated slip rates along the Puente Hills faults show significant strike-slip implying that seismic hazard of these faults may be underestimated by considering reverse-slip rates alone. Contraction at  $036^\circ$  may not be appropriate in the Puente Hills region because of resulting sinistral slip on the Whittier fault, which disagrees with paleoseismic observations; however, Whittier strike-slip rates fit paleoseismic rates under  $006.5^\circ$  contraction. Because strike-slip rates are more sensitive to contraction direction than fault intersection geometry, contraction direction should be further constrained in order to accurately assess seismic hazard on these faults.*

## **2. Introduction**

The Los Angeles basin, located at the juncture of the Peninsular and Transverse Ranges in southern California, contains a complex system of active thrust and strike-slip faults. In the northeastern Los Angeles basin, the Puente Hills blind-thrust system (PHT) is composed of three distinct east-west striking, echelon segments (Figure 1; *Shaw and Shearer, 1999*). Although

portions of the PHT system are believed to intersect the northwest-southeast striking Whittier fault, the geometry of this intersection is not constrained by available subsurface data (*Shaw et al, 2002*). The Puente Hills thrust system underlies metropolitan Los Angeles and is the source of the pure-thrust 1987 Whittier Narrows (M=6.0) earthquake (*Hauksson and Jones, 1989; Shaw and Shearer, 1999; Shaw et al, 2002*). Recently, *Dolan et al (2003)* recognized four large (> Mw 7.0) earthquakes on the PHT faults during the past 11,000 years. The occurrence of earthquakes along unrecognized or poorly characterized blind thrust faults, such as the 1987 Whittier Narrows and 1994 Northridge events, highlights the need for tighter constraints on the geometry of these structures. Furthermore, variations in intersection between the PHT and the Whittier faults yield differing fault surface areas which, along with slip rate and depth, are critical elements of predictive earthquake damage algorithms (e.g. *Wells and Coppersmith, 1994*).

Although blind faults are difficult to characterize due to a lack of surface exposure, they may be identified by seismic reflection surveys and well log data, and inferred from surface or near-surface folds. The geometry of the PHT is relatively well constrained from seismic surveys to a depth of approximately 5 km (*Shaw et al, 2002*); however, the intersection configuration between the PHT and Whittier faults remains unresolved. Although the geometry of this fault intersection is currently unconstrained, alternative kinematically viable models have been proposed for intersections between strike-slip and thrust faults (Figure 2; *Rivero and Shaw, 2000*). Variations in fault interaction within alternative intersection models may yield differing slip rates for PHT and Whittier faults. By comparing slip rates produced by mechanical models of the alternative fault configurations to geologically constrained rates, we might: 1) delineate a preferred intersection geometry; and 2) develop a complete understanding of the three-

dimensional distribution of slip on these faults. Knowledge of both fault geometry and slip rates is critical for characterization of earthquake source parameters on the PHT and Whittier faults.

This study utilizes three-dimensional mechanical models to distinguish between potential intersection geometries of the PHT and Whittier faults. The boundary element method (BEM) code Poly3D is used to model fault interaction within three kinematically plausible fault intersection configurations. Similar studies in two dimensions have assessed the mechanical compatibility of proposed fault systems and delineated a preferred configuration (*Cooke and Kameda, 2002*). Poly3D simulates deformation on non-planar fault surfaces by employing triangular elements, which provides a particularly effective means to simulate the three-dimensional interaction of non-planar or non-rectangular faults. The models use geodetically constrained remote horizontal contraction rates within the Los Angeles basin to induce fault slip. We infer that the PHT-Whittier intersection model that produces the closest match to available paleoseismic slip rates and kinematically inferred dip slip rates is the most viable model, which can subsequently be used to ascertain potential earthquake source parameters. Furthermore, the most viable model provides estimates of strike-slip rates on the unexposed PHT faults for which paleoseismic slip rates are unavailable. A secondary indicator of model viability is the global mechanical efficiency of the fault system (*Cooke and Kameda, 2002*). This efficiency assesses the effectiveness of the fault system to distribute deformation through fault slip by measuring the elastic internal work done in the system. By using two methods to assess alternative fault configurations, this study serves to test mechanical efficiency as a measure of fault system viability.

### **3.1 Geologic Setting and Fault Slip Rates**

Bounded by the Palos Verdes Peninsula to the southwest and the San Gabriel Mountains to the north, the central Los Angeles basin consists of ~5-7 km of Miocene, Pliocene, and Pleistocene strata underlain by Mesozoic metasedimentary rocks that, in the northeastern part of the basin, have been intruded by late Cretaceous granites (e.g. *Norris and Webb, 1990; Wright, 1991*).

The Los Angeles basin has been shaped by a variety of tectonic regimes during the past 18 My, including Miocene transtension and present-day transpression (e.g. *Wright, 1991; Nicholson, 1994; Ingersoll and Rumelhart, 1999*). Geodetic investigations within the Los Angeles basin estimate present-day north-south to northeast-southwest contraction (*Feigl et al, 1993; Walls et al, 1998, Argus et al, 1999; Bawden et al, 2001*). This strain, particularly within the northern basin, is accommodated along active systems of east-west oriented reverse-slip faults and southwest-northeast and northwest-southeast strike-slip faults (*Walls et al, 1998*). The concurrence of dip- and strike-slip faulting is due, in part, to the multi-stage evolution of the basin. For example, many strike-slip faults, such as the Whittier fault, formed as normal faults under earlier transtension and were later reactivated as strike-slip faults under transpression (e. g. *Ingersoll and Rumelhart, 1999; SCEC working group, 2001*).

The Puente Hills blind-thrust system (PHT) comprises three distinct, echelon blind segments (*Shaw and Shearer, 1999; Shaw et al, 2002*). From west to east, these segments are the Los Angeles, Santa Fe Springs, and Coyote Hills thrust faults (Figures 1 and 3). The geometry and slip rates of all three segments of the PHT have been inferred from seismic reflection images of fold growth structures associated with the upper fault tips (*Shaw and Suppe 1996, Shaw et al, 2002*). *Shaw et al (2002)* analyzed fold growth structures using fault-related fold theory to infer average Quaternary reverse-slip rates across the three segments of the PHT:

0.90-1.70 mm/yr for the Coyote Hills segment, 0.44-0.82 mm/yr for the Santa Fe Springs segment and 0.60-1.13 mm/yr for the Los Angeles segment. Dolan *et al* (2003) measured a minimum shorter-term (late Pleistocene-Holocene) dip-slip rate for the Santa Fe Springs segment of  $\geq 1.1$ -1.6 mm/yr.

The Whittier fault, a northwest-southeast striking reverse dextral oblique fault, forms the northeastern boundary of the Los Angeles basin and the northern extension of the Elsinore fault (Figure 1; e.g. *Ziony and Yerkes, 1985; Wright, 1991*). The ratio of Holocene reverse-slip to strike-slip on the Whittier fault is uncertain, however Holocene slip on the Whittier fault has been dominated by strike-slip motion at a rate of approximately 1-3 mm/yr in the region of the PHT, with 2-3 mm/yr as a preferred range (e.g. *Gath et al 1992; Dolan, 2001, Bjorklund et al, 2002*). Slip on the Whittier fault initiated in the mid-to late Miocene as an extensional structure, but geomorphic (e.g. stream channel offset) expression near the fault is the result of Quaternary deformation (*Wright, 1991*). We compare these geologically constrained slip rates for the PHT and Whittier faults to model results in order to validate the potential fault configurations.

### **3.2. Mechanical Efficiency**

A secondary indicator of fault configuration validity utilized in this study is the global mechanical efficiency of the fault system (e.g. *Cooke and Kameda, 2002*). This idea rests on the premise that fault systems grow to minimize the amount of work done in the system. As faults evolve, the fault surface becomes smoother by grinding processes, and new fault surfaces may be created in preferential orientations in response to accumulated elastic strain (e.g. *Scholz, 1990*). Consequently, the most mechanically efficient fault configuration is that which contains the least stored strain energy and the most fault slip.

Elastic strain accumulation within the host rock between faults is evaluated by calculating strain energy density (SED) throughout the model. SED has been used by several workers to analyze fault system deformation (e.g. *Du and Aydin*, 1993, 1995; *Cooke and Kameda*, 2002; *Savage and Cooke*, in review). SED describes the amount of work per unit volume done within the host rock (*Timoshenko and Goodier*, 1934). In three dimensions SED,  $V_o$ , is expressed in terms of principal stresses as

$$V_o = 1/2E[\sigma_1^2 + \sigma_2^2 + \sigma_3^2] - \nu/E[\sigma_1\sigma_2 + \sigma_2\sigma_3 + \sigma_1\sigma_3]$$

where  $E$  represents Young's modulus and  $\nu$  represents Poisson's ratio. Because elastic strain can be locally relieved by fault slip, SED is expected to be heterogeneous throughout active fault systems; clouds of high SED accumulate at crack tips and SED lows develop adjacent to slipping fault surfaces. We calculate SED at equally spaced points throughout each of the models, and compare the average SED of the different PHT-Whittier intersection models. The average SED, in concert with overall net slip, is used to assess the mechanical efficiency of each fault configuration. The model with the lowest average SED, and corresponding greatest net slip, has the most mechanically efficient fault system.

#### **4.1. Boundary Element Method**

Interaction of the PHT and Whittier faults is simulated using Poly3D, a three-dimensional boundary element method (BEM) code that calculates the deformation of faults within a linear elastic half-space (e.g. *Thomas*, 1993). Poly3D numerically solves the governing differential equations of continuum mechanics (e.g. *Crouch and Starfield*, 1990). Poly3D can simulate the

deformation of any three-dimensional, homogeneous, isotropic elastic body if either the tractions or displacements are prescribed on the surface of that body. Thus, the stress, strain, and displacement fields throughout the body are uniquely determined by prescribed boundary conditions (i.e. tractions or displacements). Within the models of this study, remote strain, prescribed as geodetically determined horizontal contraction (Figure 3), drives slip along fault surfaces that are weak in shear and not allowed to open. Poly3D discretizes three-dimensional faults into two-dimensional polygons, which have constant displacement continuity (*Thomas, 1994*). Triangular elements provide accurate simulation of non-planar fault surfaces (Figure 3). As a BEM code, Poly3D only requires discretization of the faults, rather than volumetric meshing of surrounding rock required by FEM. Consequently, this code facilitates easy manipulation of fault geometry (e.g. *Thomas, 1994; Willemse et al, 1996; Roering et al, 1997; Savage, 2003*).

#### **4.2. Model Set Up**

A three-dimensional model of the Puente Hills thrust system (PHT) and the Whittier fault has been constructed using published cross-sections, surface trace maps (*Wright, 1991; Shaw and Suppe, 1996; Shaw and Shearer, 1999*) and products of the Southern California Earthquake Center (SCEC) Community Fault Model (CFM) working group (*Plesch et al, 2002; <http://structure.harvard.edu/cfm/>*). Fault surfaces are composed of triangular elements, the vertices of which are prescribed by CFM workers. CFM vertex spacing varies according to resolution of data available for the fault surfaces. To increase numerical stability of the models, we have coarsened some fault meshes to maintain uniform triangular element size; however coarsening does not sacrifice the resolved non-planarity of geologic fault surfaces (Figure 3).

Rivero and Shaw (2000) outline four kinematically plausible intersection geometries between strike-slip and reverse-slip fault systems. We investigate three of these intersection scenarios (Figure 2). Because the Whittier fault predates the development of the PHT, we do not expect the fourth scenario outlined by Rivero and Shaw (2000) where the Whittier fault offsets the Coyote Hills segment of the PHT. Therefore the Coyote Hills segment either abuts the Whittier fault (model A), or extends through the Whittier fault. In the latter case, the Coyote Hills segment either offsets the Whittier fault (model C), or renders the lower surface of Whittier inactive (i.e. Coyote Hills truncates Whittier, model B). In the case of model C, we offset Whittier surface in the dip direction of Coyote Hills by a distance corresponding to the total reverse-slip reported by Shaw *et al* (2002). Although this slip is used to create the offset geometry of the Whittier fault in model C, this geometric offset in no way prescribes reverse-slip in the mechanical models; rather, modeled faults slip in response to local shear tractions on the fault. In model B, we remove the inactive portion of Whittier located in the footwall of Coyote Hills.

For this study, we prescribe remote contraction according to geodetic regional horizontal surface velocities determined within the Los Angeles basin by several workers (Figure 3; *Feigl et al*, 1993; *Argus et al*, 1999; *Bawden et al*, 2001). Because debate continues over the most appropriate contraction direction and rate, we examine fault interaction under two published rates and directions,  $72 \times 10^{-9} \text{ yr}^{-1}$  at  $006.5^\circ$  (*Feigl et al*, 1993) and  $56 \times 10^{-9} \text{ yr}^{-1}$  at  $036^\circ$  (*Bawden et al*, 2001), that may represent end-members to the range of likely contraction for the basin. By examining both conditions, we assess the sensitivity of fault interaction and slip rates to remote contraction for each proposed fault configuration.

In the area of the PHT and Whittier faults, more competent sandstones, igneous, and metamorphic rocks underlie several kilometers of sedimentary strata. Within the BEM models, prescribed homogeneous material properties should approximate the average properties of rocks underlying the Los Angeles basin. Accordingly, we prescribe a Poisson's ratio of 0.25 and Young's modulus of 30 GPa, both reasonable estimates for a combination of sandstone and gneissic bedrock (*Clark, 1966*).

The time period simulated in the models should both exceed the earthquake cycle for all faults in the models and should span a time period sufficiently short to permit quasi-static analysis. In order to encompass a reasonable earthquake recurrence interval for the Los Angeles basin faults (e.g. *Ward and Valensise, 1994; Dolan et al., 1995; 2003; McNeilan et al, 1996; Grant et al., 1997; Oskin et al., 2000*), and to ensure infinitesimal deformation, we simulate 5000 years of deformation. Although we limit our examination of slip rates to the PHT and Whittier faults, the model includes the following nearby faults to ensure accurate tectonic context: Compton, Chino, Richfield, Alhambra, Peralta Hills, Las Cienagas Upper Elysian Park, Hollywood, Raymond, Newport-Inglewood, Palos Verdes, Redondo Canyon, San Vicente, and Santa Monica (Figure 3). The geometry of these faults has been constrained by SCEC CFM workers, although the exact configuration of many southern California faults is not yet resolved. For this study, we explore variations in the intersection of the PHT and Whittier faults and leave other faults unchanged from Figure 3. The slip rates along these faults are presented in the appendix, but are not discussed in this paper.

## 5. Model Results

We investigate sensitivity of fault interaction and slip rates to three alternative intersection geometries of the PHT and Whittier faults (Figure 2). The younger Coyote Hills fault abuts the Whittier fault in model A. In models B and C, the Coyote Hills fault extends through the Whittier fault to a depth of approximately 20 kilometers (the inferred base of the seismogenic crust). The Coyote Hills fault renders the lower portion of the Whittier fault inactive in model B, and offsets Whittier in model C.

Because the modeled fault surfaces are composed of individual elements, each with constant displacement discontinuity (i.e. slip or opening), the faults have non-uniform slip rates and the net slip rate vectors are non-uniform on all faults in the models (Figure 4). In general, the slip rate is highest at the center of faults and decreases to the fault edges (Figure 4). For example, the reverse- and strike-slip rates on the Whittier fault vary both along strike at the upper trace of the fault and with depth (Figure 4). The negligible strike-slip at the eastern end of the Whittier fault results from the artificial termination of the fault within the model of the Los Angeles basin. In reality, the Whittier fault extends to the southeast, eventually merging with the Elsinore fault beyond the Los Angeles basin. Thus, strike-slip along the eastern margin is certainly non-zero. Because we have limited the model to the Los Angeles basin, both the artificial termination of faults and the exclusion of faults immediately outside the basin may distort fault slip near the edges of our study area. Despite these effects, our model results show that the greatest slip often occurs along the middle of faults and, for steeply-dipping faults that daylight, at shallow depths (e.g. Figure 4C, inset).

Slip rates approach zero at the lower tip-lines of the modeled faults because the model incorporates discrete rather than semi-infinite fault surfaces. At depths of 15-20 km within the

earth we expect the deformation associated with crustal-scale faults to transition from slip along discrete surfaces to diffuse flow. Because modeled fault surfaces terminate along lower tip lines at or above the middle crust, and do not extend through the middle crust, we do not expect the model results to exactly match average geologic slip rate magnitudes. Extension of slipping fault surfaces into the middle crust to simulate this deep diffuse flow would increase average reverse and strike slip rates, but constraining the geometry of such fault extensions is beyond the scope of this study.

The average slip rate for a fault surface can be determined by averaging strike- or reverse-slip component vectors from all individual elements. Alternatively, along strike distributions of slip-rate can be produced by averaging the slip rate vectors within successive bins that have narrow along-strike width but extend down the dip-length of the fault. One method provides a single representative slip rate for the entire fault, whereas the other provides a distribution of slip with lateral position along the fault. We use the latter to compare the model results to the interpreted reverse-slip rate distribution on PHT segments (Figure 5) and the average slip rate for the Whittier fault (Figure 6a). Because of the non-uniform distribution of slip, we expect some discrepancies between the average fault slip rates in the models and the rates determined by kinematic inferences and paleoseismology. Thus, for the PHT faults, we attempt to validate alternative intersection geometries by matching slip patterns rather than absolute slip rate magnitudes on PHT faults (Figure 5). For the Whittier fault, we compare paleoseismic slip rates to the average slip rate along the entire fault as well as modeled rates at the same location as paleoseismic studies (Figure 6).

## 5.1 Slip Rates on PHT faults

The PHT and Whittier faults have similar distributions of reverse-slip for the two horizontal contractions (Figure 5). Along each segment, reverse-slip is greatest at the center of the fault and tapers to zero at the lateral tips of the fault segments. Local peaks in reverse-slip rate for  $006.5^\circ$  contraction coincide with peaks for  $036^\circ$  contraction (Figure 5A-C). The  $036^\circ$  contraction provides consistently less reverse-slip along the PHT than the  $006.5^\circ$  contraction (Figure 5A-C), primarily because the strain rate associated with this direction is less than the rate associated with north-south contraction (Figure 4; *Bawden et al*, 2001). The reverse-slip rate on the Coyote Hills segment is most sensitive to change in the horizontal contraction direction whereas the reverse-slip rate on the Los Angeles segment changes the least with contraction direction.

We compare the model distribution of PHT slip rates to the following first-order features in the pattern of the kinematically inferred reverse-slip rate (*Shaw et al*, 2002): 1) increasing reverse-slip on the Los Angeles fault from west to east; 2) the relatively slow slip rate on the Santa Fe Springs segment compared to adjacent faults; and 3) the relatively rapid slip rate on the Coyote Hills segment. The modeled reverse-slip rates slow to the west along the Los Angeles fault, although with less asymmetry than the pattern of the inferred reverse-slip rate. For the  $036^\circ$  contraction direction, the reverse-slip rate along the Santa Fe Springs segment is slower than the Los Angeles fault; whereas the reverse-slip rate on the Santa Fe Springs segment is only slightly less than that of the Los Angeles fault under  $006.5^\circ$  contraction (Figure 5). In general, reverse-slip rates on the Santa Fe Springs and Los Angeles segments both match inferred rates more closely than modeled rates on the Coyote Hills segment.

As expected, reverse-slip rates for the three fault intersection models (A, B and C) vary primarily on the Coyote Hills segment, because the principal difference between the models is the intersection geometry of the Whittier and Coyote Hills faults (Figure 2). Models B and C better match the inferred reverse-slip rates on the Coyote Hills segment than model A, because the longer dip length of the Coyote Hills segment in these configurations increases slip so that the Coyote Hills reverse-slips faster than the Santa Fe Springs and Los Angeles segments (Figure 5B, C). With a shorter down-dip length for the Coyote Hills fault (i.e. the Coyote Hills segment abuts the Whittier fault, model A), the Coyote Hills and Santa Fe Springs segments have comparable slip rates, in contrast to the relatively fast slip rates on the Coyote Hills segment inferred from structural relief. This result suggests that models B and C are preferred over A, and that the Coyote Hills segment does not abut the Whittier fault. Models B and C have a similar reverse-slip pattern so that we cannot further constrain the geometry of the fault intersection by comparison to the inferred reverse-slip rate distribution along the PHT fault segments.

The three-dimensional mechanical models provide a complete picture of the net slip vector along the PHT fault segments, which can be expressed as the ratio of average strike- to reverse-slip (Table 1). Large slip ratios ( $\gg 1$ ) indicate primarily strike-slip, whereas low ratios ( $\ll 1$ ) indicate primarily dip slip; ratios near one suggest highly oblique slip on faults. Although the obliquity of slip on the PHT does not vary greater with alternative fault intersection configurations, strike- to reverse-slip ratios are highly sensitive to the contraction direction. The Santa Fe Springs and Coyote Hills faults undergo primarily reverse-slip under  $006.5^\circ$  contraction, but under  $036^\circ$  contraction these faults experience significant component of strike-slip (Table 1). In contrast, the Los Angeles fault experiences a significant component of strike-

slip under  $006.5^\circ$  contraction and much less strike-slip under  $036^\circ$  contraction. Interestingly, the Los Angeles fault experiences a change in sign in strike-slip sense under  $006.5^\circ$  and  $036^\circ$  contraction. The ratios of strike- to reverse-slip suggest that regardless of contraction direction, portions of the Puente Hills Thrust system may experience significant strike-slip under all kinematically viable fault intersection configurations. This implies that seismic hazard estimates for these faults based on reverse-slip alone may be inadequate and the strike-slip contribution should be further constrained.

## **5.2. Slip rate on Whittier Fault**

All three mechanical fault intersection models under  $006.5^\circ$  and  $72 \times 10^{-9} \text{ yr}^{-1}$  remote contraction yield greater strike-slip rates along the Whittier fault than  $036^\circ$  and  $56 \times 10^{-9} \text{ yr}^{-1}$  (Figure 6). Furthermore, under  $036^\circ$  remote contraction, the modeled Whittier fault has a sinistral slip sense (Figures 4 and 6) in disagreement with geologic observations (*Gath et al*, 1992). The source of this slip sense reversal can be understood with reference to Figure 3. Contraction at  $006.5^\circ$  resolves a large component of dextral slip on the Whittier fault, whereas contraction at  $036^\circ$  resolves a small sinistral component of slip on this fault. These results suggest that  $036^\circ$  contraction cannot produce slip on the Whittier fault that resembles geologic observations. Because this slip sense reversal casts doubt on the appropriateness of  $036^\circ$  contraction in this region, we limit the following analysis to model results under  $006.5^\circ$  contraction.

The average strike-slip rate along the Whittier fault in models A and C, with the Coyote Hills abutting (model A) and crossing (model C) the Whittier fault show slightly better match to the paleoseismic slip rates than model B (Figure 6A). Because the paleoseismic rates are

measured at a specific site along the fault trace, we compare the near-surface strike-slip with paleoseismic observations in Figure 6B. At the approximate location of the paleoseismic investigation of Gath *et al* (1992), models A and C yield  $\sim 1$  mm/yr near surface strike-slip rates, whereas model B has  $\sim 0.8$  mm/yr near surface strike-slip rate. These rates are close to the average strike-slip rate on the entire Whittier fault, which ranges from  $\sim 0.9$  to  $1.0$  mm/yr (Figure 6A). Because the near surface strike-slip rate varies with position along the trace of the Whittier fault (Figure 6B), the site chosen by Gath *et al* (1992) appears to be the most suitable for determining representative strike-slip rate. The greater strike-slip rates of models A and C yield slightly better match to paleoseismic rates than model B (Figure 6A, B). Because model A was ruled out due to the excessively low reverse-slip rate on the Coyote Hills fault, the comparison of strike-slip on the Whittier fault provides a slight preference for model C, with Whittier active to the base of the seismogenic zone.

Bjorklund *et al* (2002) contend that Quaternary deformation on the Whittier fault has been dominated by reverse-slip along the central and northwest segments of the Whittier fault, although significant strike-slip displacement may have occurred on the southeast portion of the fault. Three-dimensional mechanical model results indicate that the strike- to reverse-slip ratio is slightly greater than 1:1 on the northwest portion of the Whittier fault, but this ratio increases to 6:1 to the southeast of the study area of Bjorklund *et al* (2002; Figure 6 C). These results are consistent with a decrease in the reverse-slip component to the southeast as per the assessment of Bjorklund *et al* (2002). We ascribe this change to both variations of strike and dip along the central section of the Whittier fault and interaction with the Chino fault. The Whittier fault surface changes strike from a roughly east-west (reverse-slip favorable orientation) at the intersection with the Coyote Hills fault to northwest-southeast (relatively strike-slip favorable

orientation) east of this intersection. Furthermore, at the intersection of the Whittier and Chino faults, reverse-slip along the Chino fault accommodates regional contraction thereby decreasing reverse slip on the Whittier fault (Figure 4). The overall ratio of strike- to reverse-slip calculated from the average slip rate across the entire fault is approximately 2:1 under  $006.5^\circ$  contraction, suggesting that strike-slip dominates the overall deformation of the Whittier fault (Table 1).

### **5.3. Mechanical Efficiency**

Fault slip relieves stored elastic strain in the host rock so that, under identical remote strains, models with faster overall slip rates have greater mechanical efficiency than models with relatively low slip rates. To assess the relative mechanical efficiency of the proposed fault intersections, we normalize the average strain energy density (SED) for models A, B, and C to a model with no fault surfaces. The normalized average SED values of the fault models are less than one because the external work acting on the system goes into both elastic deformation of the host rock and fault slip, whereas the less efficient fault-less models only strain the host rock. Moreover, the average SED is calculated for the region immediately surrounding the PHT and Whittier faults rather than for the entire basin. This reduces the apparent SED variations due to changing conditions along other faults.

The expected correlation of average SED to average net slip on all faults is consistent for all intersection models; increases in average net slip accompany drops in average SED (Figure 7). For both contraction directions, model B faults slip the least and produce the highest SED, indicating that this model is the least efficient of the PHT-Whittier intersection scenarios. Model C, with the Coyote Hills segment offsetting the Whittier fault, has both the highest average net slip rate for all faults in the model and the lowest average SED under both  $006.5^\circ$  and  $036^\circ$

contraction (Figure 7). This suggests that the model with the Coyote Hills segment offsetting the Whittier fault, and the Whittier fault extending to the base of the seismogenic zone, has the greatest mechanical efficiency. Thus, the most mechanically efficient model also has the best match of modeled slip rates to geologic rates.

## 6.1 Discussion

Left-lateral slip on the modeled Whittier fault under  $036^\circ$  contraction casts skepticism on the viability of this contraction direction in the eastern Los Angeles basin. This rate, which corrects for groundwater effects on surface velocity, seems unsuitable for the Puente Hills region although  $N36E$  contraction may be appropriate in other portions of the Los Angeles basin. Slip sense and slip rates under  $006.5^\circ$  contraction better resemble geologic observations on the PHT and Whittier faults than  $N36^\circ E$ . Contraction directions intermediate to  $N6.5^\circ E$  and  $N36E$  will have slip rates intermediate to those presented. In a study with 25 faults of the Los Angeles basin, Griffith and Cooke (in prep) find that of the variety of proposed tectonic boundary conditions for the region, north-south principal contraction with zero east-west strain best matches geologic slip styles across the basin.

Under the preferred boundary conditions of this study,  $0006.5^\circ$  contraction, a comparison of modeled slip rates on the PHT faults with kinematic inferences region indicates that the Coyote Hills segment of the PHT extends to a depth of 17-20 km. Comparison of model strike-slip on the Whittier fault to paleoseismic rates gives a slight preference for a model in which the Coyote Hills fault offsets the Whittier fault, and the Whittier fault is active to the base of the seismogenic zone. The extension of the Coyote Hills fault north of and below the Coyote Hills-Whittier intersection is consistent with findings of several workers. First, seismicity associated

with the 1987 Whittier Narrows event on the adjacent Santa Fe Springs segment extended north of the Whittier fault (e.g. *Shaw et al*, 2002). Also, uplift rates in the Puente Hills are nearly equal to the north and south of the Whittier fault, implying that both sides of the Whittier fault are uplifted together within the hanging wall of the PHT (e.g. *Gath*, 2000); the abutment of the Coyote Hills segment against the Whittier fault would produce asymmetric uplift across the Whittier fault. The mechanical efficiency analyses support the preference of the Whittier fault extending to the base of the seismogenic crust. However, the configuration with the Whittier fault inactive in the footwall of the Coyote Hills segment is still permissible with the available constraints.

Results of this study have important implications for earthquake hazard assessment. First, the PHT faults experience significant strike-slip motion under all modeled conditions, and strike-slip is the model parameter most sensitive to contraction direction. For the preferred model, the ratio of strike-slip to reverse-slip for the Los Angeles, Santa Fe Springs and Coyote Hills faults is 0.43, 0.08 and 0.29, respectively. This strike-slip on the PHT conflicts with the thrust sense of movement of the 1987 Whittier Narrows earthquake, which occurred on the Santa Fe Springs segment (*Shaw and Shearer*, 1999). Apparent strike-slip on the PHT could be reduced by details of fault topology not considered here. For example, dip direction corrugations (e.g. *Carena and Suppe* 2002) may inhibit oblique slip and promote reverse slip. Conservative seismic hazard assessment for the Los Angeles segment, and to a lesser degree the Coyote Hills segment, of the PHT should therefore focus on both strike-slip and reverse-slip rates. Furthermore, probable earthquake magnitudes for the Coyote Hills fault should be based on the fault area extending to the base of the seismogenic zone (17-20 km). Consequently, the potential of this fault to produce larger and/or more frequent earthquakes is greater than a hazard

assessment using a configuration in which the Whittier fault truncates the Coyote Hills segment. Although we cannot resolve with certainty the extent of the active Whittier fault from this study, the probable earthquake source area for the Whittier fault should extend to the base of the seismogenic crust in order to be conservative.

## **6.2. Implications of slip distribution to paleoseismic investigations**

If natural faults display the variability of slip distribution seen in Figure 4, determination of a slip rate for the entire fault from trenching at a particular location along the fault trace may not accurately represent the average slip rate for the entire fault. Depending on location, the slip rate at a single point on the fault may under- or overestimate the average fault slip. For faults with greatest slip at shallow depths (e.g. Whittier, Chino, Palos Verdes, Santa Monica, etc), paleoseismic estimates likely overestimate the average slip rate. Moreover, slip rates kinematically determined from fold structures above the PHT faults primarily reflect slip rates on the upper portion of the PHT faults. These may or may not reflect the slip rates at deeper levels. The mechanical models show relatively low slip rate along PHT faults at shallow levels (Figure 4).

## **6.3. Slip-rate Discrepancies on PHT and Whittier faults**

Although reverse-slip rates of the preferred fault intersection model generally show good agreement with kinematically inferred long-term rates of the Los Angeles and Santa Fe Springs faults, the inferred long-term rates on the Coyote Hills fault are significantly greater than the adjacent Los Angeles and Santa Fe Springs segments (Figure 5A-C), a pattern not observed in our models. This sharp increase in reverse-slip rate from the Santa Fe Springs fault to Coyote

Hills fault inferred from structural relief cannot be explained by changes in remote contraction orientation nor by interaction with the Whittier fault, both factors incorporated into our models. Utilizing overall softer or stiffer rock properties would alter the slip magnitude, but would not change the relative pattern of slip. This discrepancy should be explored further by investigation of secondary faulting and possible lateral heterogeneities in material properties.

Another discrepancy is the poor fit of model results for the slip rate distribution on the western Los Angeles fault segment. Inferred rates indicate that the slip rate progressively increases from west to east on the Los Angeles segment (Figure 5A-C). The modeled reverse-slip rates do not increase as sharply as the inferred rates. The Los Angeles segment intersects the San Vicente and Raymond faults on its western side; interaction with these faults may explain this discrepancy and should be investigated with alternative intersection scenarios. Furthermore, the structural relief on the western Los Angeles fault may be younger than the eastern portion of the fault, yielding artificially low slip rates (*J. Shaw*, pers. comm., 2003). Lateral propagation of fault systems may result in asymmetric distributions of cumulative slip (greater slip along older portion) that produce asymmetric structural relief. Western propagation of the PHT could account for the asymmetric slip rates along the Los Angeles segment as well as the asymmetry across the three segments of the Puente Hills system (*J. Shaw*, pers. comm., 2003). The inference of westward propagation of the Puente Hills system is further supported by a three-dimensional investigation of lateral fault propagation using three different measures of propagation propensity (*Olson and Cooke*; in review).

Increases in regional contraction rate would increase the modeled slip rates on the PHT and Whittier faults. Argus *et al* (1999) report horizontal velocities between the Jet Propulsion Laboratory (JPL) and the Palos Verdes (PV) benchmarks of  $\sim 5.6$  mm/yr. This rate results in a

contraction rate of  $100 \times 10^{-9} \text{ yr}^{-1}$ , significantly greater than contraction applied to models in this study. These higher strain rates will result in faster reverse-slip rates along the PHT and Whittier faults.

Near surface strike-slip rates on the modeled Whittier fault under  $006.5^\circ$  contraction are slower than geologic rates (Figure 6B). Artificial basal and lateral fault terminations reduce the average and maximum strike-slip rates. Under similar boundary conditions, a model that incorporates the Elsinore fault as the southern extension of the Whittier fault produces  $\sim 1.5$  mm/yr average strike-slip rate on the Whittier fault, in closer agreement with geologic estimates (*Griffith and Cooke, in prep*). Extending the Whittier fault down-dip into the middle crust would also increase average and near surface slip rates.

## 7. Conclusion

This study has evaluated among a set of plausible fault models for the intersection of the Puente Hills thrust-system and Whittier fault by: 1) comparing slip rates from the three-dimensional mechanical models of interacting faults with available paleoseismic data and kinematic inferences; and 2) analyzing the overall internal work within the fault system models which allows assessment of the relative mechanical efficiency of the models. Comparison of model results consistently indicates that the most viable intersection geometry is one in which the Coyote Hills segment of the Puente Hills thrust extends through and offsets the Whittier fault. Furthermore, the strike-slip rates on Whittier and the strain energy density results suggest that the active Whittier fault extends to the base of the seismogenic zone, although a configuration in which the Whittier fault is inactive in the footwall of the Coyote Hills segment

is still permissible. The correspondence of low strain energy density, which indicates greater mechanical efficiency, and best-fit of geologic slip-rates for the model in which the Coyote Hills segment offsets the Whittier fault lends support to the application of mechanical efficiency to fault validation studies. Average strain energy density can be an effective diagnostic tool for geometry validation because this parameter is easily calculated and represents overall behavior of the fault system.

A  $006.5^\circ$  contraction across the basin produces slip rates that are more consistent with paleoseismic and kinematically inferred rates than does a contraction direction of  $036^\circ$ . In particular, the sinistral slip along the Whittier fault produced by  $036^\circ$  contraction is opposite to the observed dextral slip on this fault, suggesting that this contraction direction is problematic in this region.

The three-dimensional mechanical models provide a complete description of slip distribution on faults. The variability of modeled slip rates on individual fault patches implies that slip rates measured via surface trenches and inferred from fold structures are not guaranteed to accurately represent the overall slip rates of faults. Theoretical slip maps such as Figure 4 can be used to choose suitable locations for paleoseismic investigation. Furthermore, the results of this study indicate that strike-slip motion may be significant on PHT faults and should be considered in predictive earthquake hazard algorithms. Hazard analysis limited to reverse slip on these faults may underestimate earthquake risk. Moreover, the sensitivity of strike-slip on both the PHT and Whittier faults to contraction direction highlights the need for further investigation of the overall contraction direction in the Los Angeles basin.

The SCEC Community Fault Model database contains three-dimensional meshed faults fault surfaces throughout the Los Angeles basin and, with variable resolution, throughout all of

southern California (<http://structure.harvard.edu/cfma>). Within the database, several alternative geometries have been provided for under-constrained fault surfaces, and intersection geometries of many faults are still largely unresolved. The methodology implemented in this study provides a quantitative means to assess three-dimensional mechanical fault interaction between faults with complex geometries and non-planar surfaces, and can be applied to future fault geometry validation studies. The relatively well-constrained geology of the Los Angeles basin has served as an excellent proving ground for our methodology, yielding important insights for seismic hazard assessment.

### **Acknowledgements**

This manuscript was greatly improved by reviews by John Shaw, James Dolan and Roland Burgmann as well as discussions with Erik Olson, Jon Lewis and Kathy Staffier. This research was supported by the Southern California Earthquake Center. SCEC is funded by NSF Cooperative Agreement EAR-0106924 and USGS Cooperative Agreement 02HQAG0008. The SCEC contribution number for this paper is 735.

## 8. References

- Argus, D. F., M. D. Heflin, A. Donnellan, F. H. Webb, D. Dong, K. J. Hurst, G. A. Jefferson, M. Lyzenga, M. Watkins and J. F. Zumberge, (1999). Shortening and thickening of metropolitan Los Angeles measured and inferred by using geodesy. *Geology*, **27**: 703-706.
- Bawden, G. W., W. Thatcher, R. S. Stein, K. W. Hudnut and G. Peltzer, (2001). Tectonic contraction across Los Angeles after removal of groundwater pumping effects. *Nature*, **412**: 812-815.
- Birch, F., (1966). Compressibility; elastic constants, in *Handbook of Physical Constants*. In: S. P. Clark (Editor), *Handbook of Physical Constants*. Geological Society of America, New York, NY, pp. 587.
- Bird, P. and X. Kong, (1994). Computer simulations of California tectonics confirm very low strength of major faults. *Geol. Soc. Am. Bull.*, **106**(2): 159-174.
- Bjorklund, G. W. and K. Burke, (2002). Four-dimensional analysis of the inversion of a half-graben to form the Whittier fold-fault systems of the Los Angeles basin. *J. Struct. Geol.*, **24**: 1369-1397.
- Carena, S. and J. Suppe, (2002). Three-dimensional imaging of active structures using earthquake aftershocks: the Northridge Thrust, California. *J. Struct. Geol.*, **24**: 887-904.
- Clark, M. M., K. K. Harms, J. J. Lienkaemper, D. S. Harwood, K. R. Lajoie, J. A. Matti, M. J. Perkins, R. V. Rymer, R. V. Sarna-Wojcicki, R. V. Sharp, J. D. Sims, J. C. Tinsely and J. I. Ziony, (1984). Preliminary slip-rate table for late Quaternary faults of California. *U. S. Geol. Surv. Open-File Rept.*, **12**: 84-106.
- Contreras, J., M. Anders and C. Scholtz, (2000). Growth of a normal fault system: observations from the Lake Malawi basin of the east African rift. *J. Struct. Geol.*, **22**: 159-168.
- Cooke, M. L. and A. Kameda, (2002). A two-dimensional analysis using mechanical efficiency. *J. Geophys. Res.*, **107**(B7): doi:10.1029/2001JB000542.
- Crouch, S. L. and A. M. Starfield, (1990). *Boundary Element Methods in Solid Mechanics*. Unwin Hyman, Boston, 322 pp.
- Dolan, J. F., K. E. Sieh, T. K. Rockwell, R. S. Yeats, J. Shaw, J. Suppe, G. Huftile and E. Gath, (1995). Prospects for larger or more frequent earthquakes in greater metropolitan Los Angeles. *Science*, **267**: 188-205.

- Dolan, J. F., S. A. Christofferson and J. H. Shaw, (2003). Recognition of Paleoearthquakes on the Puente Hills Blind Thrust Fault, California. *Science*, **300**(5616): 115-118.
- Du, Y. and A. Aydin, (1993). The maximum distortional strain energy density criterion for shear fracture propagation with applications to the growth paths of en echelon faults. *Geophys. Res. Let.*, **20**(11): 1,091-1,094.
- Du, Y. and A. Aydin, (1996). Is the San Andreas big bend responsible for the Landers earthquake and the eastern California shear zone? *Geology*, **24**(3): 219-222.
- Feigl, K. L., D. C. Agnew, Y. Bock, D. Dong, A. Donnellan, B. H. Hager, T. A. Herring, D. D. Jackson, T. H. Jordan, R. W. King, K. M. Larsen, M. H. Murray, Z. Shen and F. H. Webb, (1993). Space geodetic measurement of crustal deformation in Central and Southern California. *J. Geophys. Res.*, **98**(12): 21,677-21,712.
- Gath, E. M., T. Gonzalez and T. Rockwell, (1992). Slip Rate of the Whittier fault based on 3-D trenching at Brea, Southern California. *Abstracts with Programs, Geol. Soc. Am.*, **24**(5): 26.
- Grant, L. B., J. T. Waggoner, T. K. Rockwell and C. von Stein, (1997). Paleoseismicity of the north branch of the Newport-Inglewood fault zone in Huntington Beach, California, from cone penetrometer test data. *Bull. Seism. Soc. Am.*, **87**(2): 277-293.
- Griffith and Cooke in preparation, How sensitive are fault slip rates in the Los Angeles basin to tectonic boundary conditions?, intended for BSSA.
- Harris, R. A., (1998). Stress triggers, stress shadows, and implications for seismic hazard, Introduction to the special issue. *J. Geophys. Res.*, **103**: 24,247-24,358.
- Hauksson, E., (1990). Earthquakes, faulting, and stress in the Los Angeles basin. *J. Geophys. Res.*, **95**(B10): 15,365-15,394.
- Ingersoll, R. V. and P. E. Rumelhart, (1999). Three-stage evolution of the Los Angeles basin, Southern California. *Geology*, **27**(7): 593-596.
- Johnson, H., (1995). Dense GPS profiles: can they distinguish between LA fault models? *EOS*, **76**(46): 142.
- Maerten, L., E. J. M. Willemsse, D. D. Pollard and K. Rawnsley, (1999). Slip distributions on intersecting normal faults. *J. Struct. Geol.*, **21**: 259-271.
- Maerten, L., (2002). Effects of local stress perturbation on secondary fault development. *Journal of Structural Geology*, **24**(1): 145-153.
- Nicholson, C., C. C. Sorlien, T. Atwater, J. C. Crowell and B. P. Luyendyk, (1994). Microplate capture, rotation of the western Transverse Ranges, and initiation of the San Andreas

- transform as a low-angle fault system. *Geology*, **22**: 491-495.
- Olson, E. and M. Cooke in review, Assessing measures of fault growth by simulating evolution of the Puente Hills Thrust system, Los Angeles, *Journal of Structural Geology*.
- Oskin, M., K. Sieh, T. K. Rockwell, G. Miller, P. Guptill, M. Curtis, S. McArdle and P. Elliot, (2000). Active parasitic folds on the Elysian Park anticline; implications for seismic hazard in central Los Angeles, California. *Geol. Soc. Am. Bull.*, **112**(5): 693-707.
- Petersen, M. D. and S. G. Wesnousky, (1994). Fault slip rates and earthquake histories for active faults in Southern California. *Bull. Seism. Soc. Am.*, **84**(5): 1,608-1,649.
- Petersen, M. D., C. H. Cramer, W. A. Bryant, M. S. Reichle and T. R. Topozada, (1996). Preliminary seismic hazard assessment for Los Angeles, Ventura, and Orange Counties, California, affected by the 17 January 1994 Northridge earthquake. *Bull. Seism. Soc. Am.*, **86**(1B): S247-S261.
- Plesch, A. and J. H. Shaw, (2001). 3-D fault architecture of the Los Angeles basin, CA, *AAPG Annual Meeting Expanded Abstracts*, 2001, 158-159.
- Rivero, C. and J. H. Shaw, (2000). Structural model of thrust inversion of low-angle normal fault systems; the Oceanside San Diego Faults, Inner California Borderland, USA,. *Annual Meeting Expanded Abstracts, Am. Assoc. Petroleum Petrologists*, **125**.
- Roering, J. J., M. L. Cooke and D. D. Pollard, (1997). Why blind thrust faults do not propagate to the earth's surface: Numerical modeling of coseismic deformation associated with thrust-related anticlines. *J. Geophys. Res.*, **102**: 11,901-11,912.
- Savage, J. C. and M. Lisowski, (1998). Viscoelastic coupling model of the San Andreas Fault along the big bend, southern California. *J. Geophys. Res.*, **103**(B4): 7,281-7,292.
- Savage, H., (2003). Three-dimensional interaction among fault-cored folds. Master's Thesis, University of Massachusetts, Amherst, Massachusetts, 108 pp.
- Savage, H. M. and M. L. Cooke, (in press). An investigation into the role of fault interaction on fold patterns. *J. Struct. Geol.*
- SCEC working group, Dolan, J. F., E. M. Gath, L. B. Grant, M. Legg, S. Lindvall, K. Mueller, M. Oskin, D. F. Ponti, C. M. Rubin, T. K. Rockwell, J. H. Shaw, J. A. Treiman, C. Walls and R. S. Yeats, (2001). Active Faults in the Los Angeles Metropolitan Region. *SCEC Spec. Pub. Series*, **1**.
- Schneider, C. L., C. Hummon, R. S. Yeats and G. L. Huftile, (1996). Structural evolution of the northern Los Angeles basin, California, based on growth strata. *Tectonics*, **15**(2): 341-355.

- Scholz, C. H., (2002). *The Mechanics of Earthquakes and Faulting*. Cambridge University Press, New York, 471 pp.
- Shaw, J. H. and J. Suppe, (1996). Earthquake hazards of active blind-thrust faults under the central Los Angeles basin, California. *J. Geophys. Res.*, **101**: 8,623-8,642.
- Shaw, J. H. and P. M. Shearer, (1999). An elusive blind thrust beneath metropolitan Los Angeles. *Science*, **283**: 1,516-1,518.
- Shaw, J. H., A. Plesch, J. Dolan, T. Pratt and P. Fiore, (2002). Puente Hills blind-thrust system, Los Angeles, California. *Bull. Seism. Soc. Am.*, **92**(8).
- Thomas, A. L., (1993). Poly3D: A three dimensional, polygonal element, displacement discontinuity boundary element computer program with applications to fractures, faults, and cavities in the earth's crust. Master's Thesis, Stanford University, Stanford, CA, 52 pp.
- Timoshenko, S. P. and J. N. Goodier, (1934). *Theory of Elasticity*. McGraw Hill, New York.
- Walls, C., T. Rockwell, K. Mueller, Y. Bock, S. Williams, J. Pfanner, J. Dolan and P. Fang, (1998). Escape tectonics in the Los Angeles metropolitan region and implications for seismic risk. *Nature*, **364**: 356-360.
- Wells, D. L. and K. J. Coppersmith, (1994). New empirical relationships among magnitude, rupture length, rupture width, rupture area, and surface displacement. *Bull. Seism. Soc. Am.*, **84**: 974-1002.
- Willemsse, E. J. M., D. D. Pollard and A. Aydin, (1996). Three-dimensional analyses of slip distributions on normal fault arrays with consequences for fault scaling. *J. Struct. Geol.*, **18**(2/3): 295-309.
- Willemsse, E. J. M., (1997). Segmented normal faults: Correspondence between three-dimensional mechanical models and field data. *J. Geophys. Res.*, **102**(B1): 675-692.
- Wright, T. L., (1991). Structural geology and evolution of the Los Angeles basin, California. In: K. T. Biddle (Editor), *Active Margin Basins*, pp. 35-134.

9. Table 1

---

Fault	<i>Model A</i>		<i>Model B</i>		<i>Model C</i>	
	N6.5E	N36E	N6.5E	N36E	N6.5E	N36E
Santa Fe Springs	0.08	0.64	0.12	0.59	0.08	0.61
Coyote Hills	0.27	0.97	0.26	0.76	0.29	0.72
Los Angeles	0.43	0.15	0.41	0.14	0.43	0.15
Whittier	2.11	0.42	2.81	0.39	2.05	0.46

---

## 10. Figure Captions

Figure 1: Location of Los Angeles basin. Surface traces of major faults, including Santa Monica, Hollywood, Raymond, Whittier, Newport-Inglewood, Palos Verdes, and Redondo Canyon (RCF), represented by gray lines (from *Wright*, 1991). The Puente Hills blind-thrust system is represented by structure contours (modified from *Shaw et al*, 2003).

Figure 2: Three kinematically plausible intersection configurations for the Whittier (WF) and Coyote Hills (CH) faults. A) Coyote Hills abuts the Whittier fault. B) Coyote Hills truncates the Whittier fault and the lower Whittier fault in the footwall of Coyote Hills is inactive. C) Coyote Hills offsets the Whittier fault, and Whittier remains active to the base of the seismogenic zone (modified from *Rivero and Shaw*, 2000).

Figure 3: Map view projection of three-dimensional geometry of modeled faults includes Los Angeles (LA), Santa Fe Springs (SFS), Coyote Hills (CH), Whittier (WF) Santa Monica (SM), Hollywood (HW), Raymond (RF), San Vicente (SV), Las Cienagas (LC), Alhambra (AF), Richfield (RH), Peralta Hills (PH), Chino (CN), Compton (CF), Newport-Inglewood (NIF), Redondo Canyon (RCF), and Palos Verdes (PV). The line overlapping PV represents the coastline. By utilizing triangular elements (e.g. LA in figure), non-planar faults can be accurately represented. Geodetically determined remote contraction drives fault slip in the models. Alternative

Coyote Hills-Whittier fault intersection geometries are deformed according to two proposed horizontal contraction velocities: 1) Feigl *et al* (1993) found  $72 \times 10^{-9} \text{ yr}^{-1}$  at  $006.5^\circ$  whereas 2) Bawden *et al* (2001) found  $56 \times 10^{-9} \text{ yr}^{-1}$  at  $036^\circ$  by removing the effects of ground subsidence in Los Angeles from the geodetic signal. Argus *et al* (1999) and Walls *et al* (1998) found similar contraction direction as Feigl *et al* (1993) and faster contraction rates. Arrows illustrate maximum shortening direction, while arrow size indicates relative magnitude. The 3-D geometry can be viewed as a virtual reality modeling language (VRML) file at <http://www.geo.umass.edu/faculty/cooke/topics/LA.html>

Figure 4: Slip-rate maps for two of the six models investigated in this study. A) and C) illustrate three-dimensional slip rate distributions for model C under  $006.5^\circ$  and  $72 \times 10^{-9} \text{ yr}^{-1}$  contraction. B) and D) represent slip rate distribution for model C under  $036^\circ$  and  $56 \times 10^{-9} \text{ yr}^{-1}$  contraction. The region of greatest reverse-slip on the Coyote Hills fault, under both contraction directions lies north (down-dip) of Whittier (A and B). Under  $036^\circ$  contraction, the sense of strike-slip changes from dextral to sinistral on both the Whittier and Los Angeles faults. Side view of the Whittier fault illustrates variable strike- and reverse-slip rates on Whittier along strike and down dip (inset). For three-dimensional, virtual reality models (VRML) of all slip maps, see <http://www.geo.umass.edu/faculty/cooke/topics/LA.html>

Figure 5: Comparison of modeled reverse-slip distribution across PHT faults to rates inferred from structural relief assuming a fault dip of  $27^\circ$  (Shaw *et al*, 2003). Reverse-slip rate for Los Angeles (LA), Santa Fe Springs (SFS), and Coyote Hills (CH) faults are represented by gray dotted curves for models under  $006.5^\circ$  contraction of  $72 \times 10^{-9} \text{ yr}^{-1}$  and dashed curves for models under contraction of  $56 \times 10^{-9} \text{ yr}^{-1}$  at  $036^\circ$ . The pattern of slip for models B and C show closer fit to inferred rates than model A because the longer Coyote Hills segment yields greater slip rate to more closely match the kinematically inferred pattern. Santa Fe Springs and Coyote Hills faults are more sensitive to changes in contraction magnitude/direction than the Los Angeles fault. Kinematic inferences of slip rate from structural relief were not made along the eastern portion of Coyote Hills.

Figure 6: A) Average strike-slip rate on the entire Whittier fault. Gray area indicates the range of paleoseismic strike-slip rates determined by Gath *et al* (1992). Dark gray region indicates the preferred paleoseismic strike-slip rate range. Positive values indicate dextral slip; negative values represent sinistral slip. Error bars are one standard deviation from the average. Strike-slip along Whittier is more sensitive to contraction direction than fault geometry. B) Near surface dextral strike-slip rates from west to east along the Whittier fault (under  $006.5^\circ$ ,  $72 \times 10^{-9} \text{ yr}^{-1}$  contraction). Gray bar indicates the approximate location of the study site

of Gath *et al* (1992) where the range of average strike-slip of 1-3 mm/yr (2-3 mm/yr preferred) was determined. C) Average reverse-slip and strike-slip rates along the Whittier fault (model C under  $006.5^\circ$  and  $72 \times 10^{-9} \text{ yr}^{-1}$  contraction) averaged along the entire depth. The obliquity of slip along the Whittier fault changes within the southeastern portion of the Bjorklund study area. The modeled Whittier fault surface extends approximately 20km southeast of the study area of Bjorklund *et al* (2002).

Figure 7: Normalized average strain energy density (SED) and average net slip on all modeled faults for alternative fault intersection geometries under  $006.5^\circ$  and  $036^\circ$  remote horizontal contraction. SED for each model is normalized to a faultless model under corresponding remote contraction. Error bars are one standard deviation from average values. Model C has the greatest mechanical efficiency

Table 1: Strike-slip to reverse-slip ratios of PHT and Whittier faults for all six fault intersection models evaluated in this study.

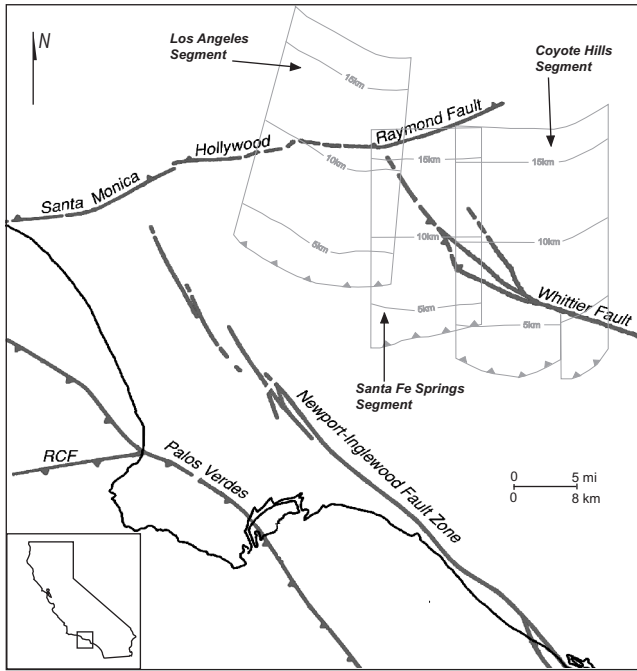


Figure 1

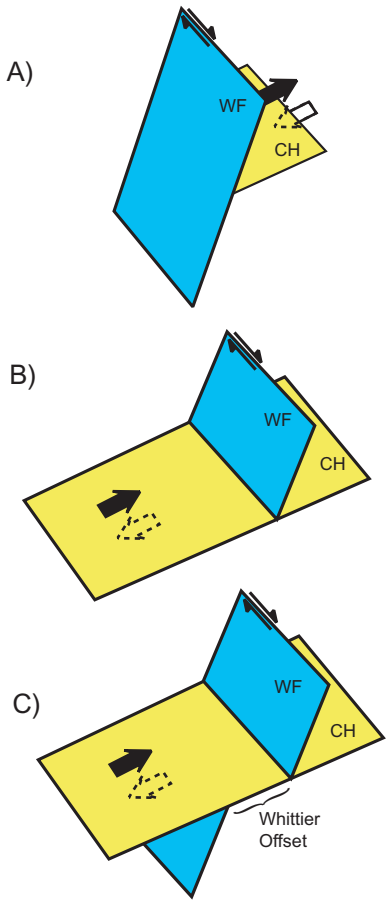


Figure 2

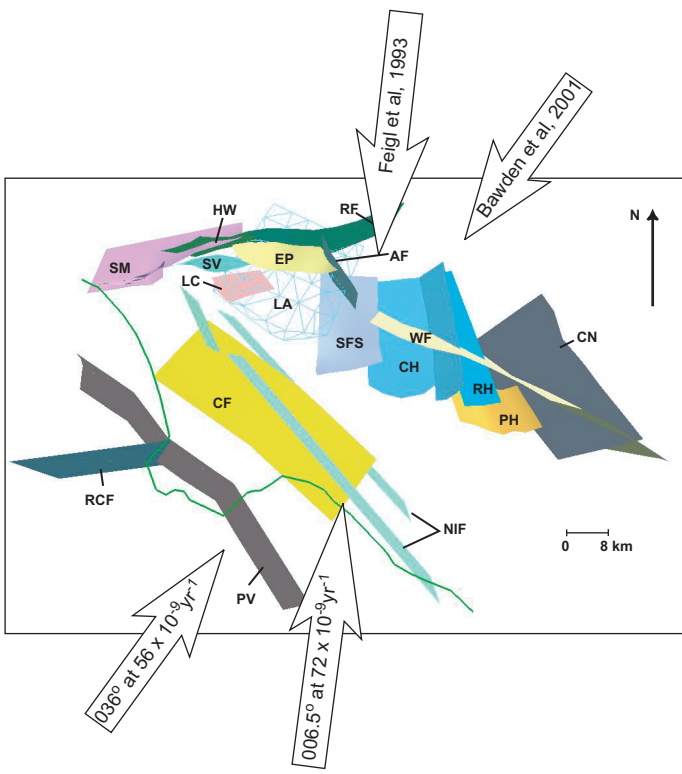
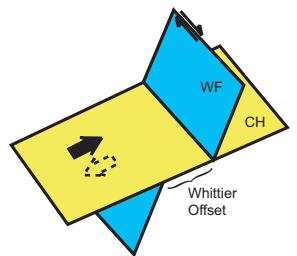
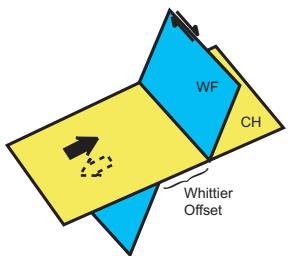
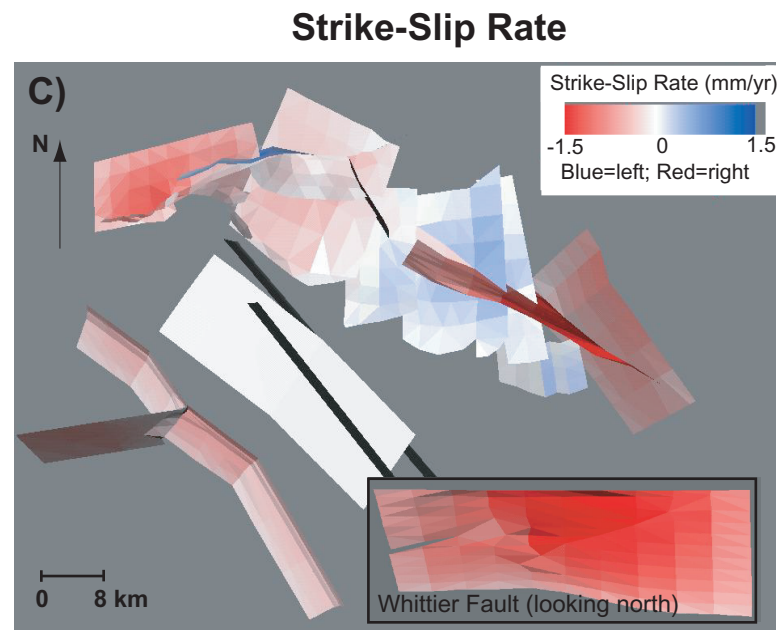
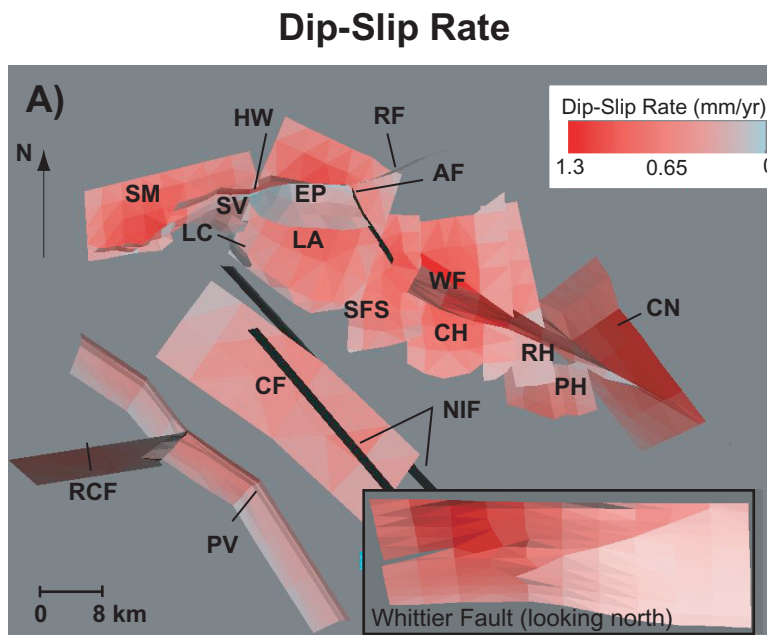


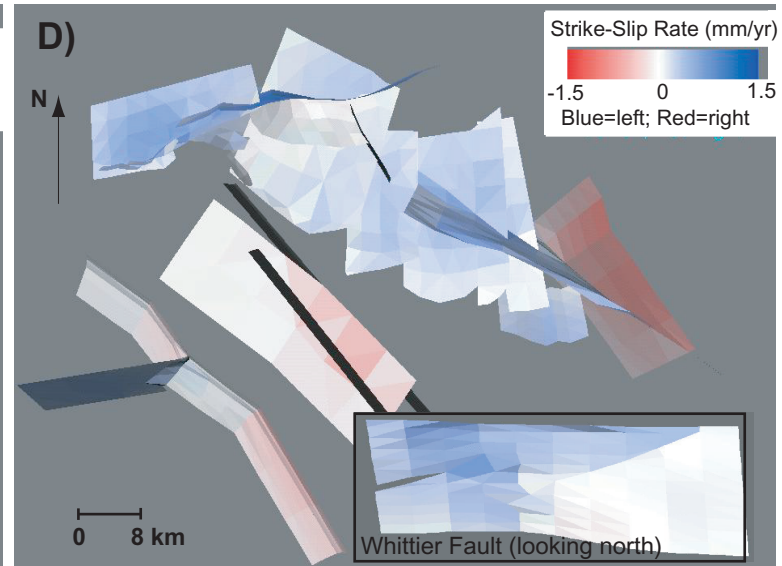
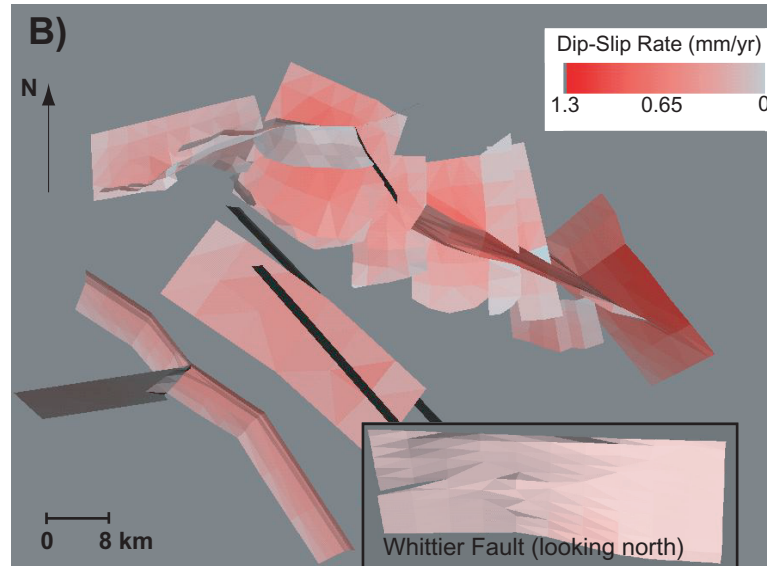
Figure 3



Model C  
 $006.5^\circ, 72 \times 10^{-9} \text{yr}^{-1}$



Model C  
 $036^\circ, 56 \times 10^{-9} \text{yr}^{-1}$



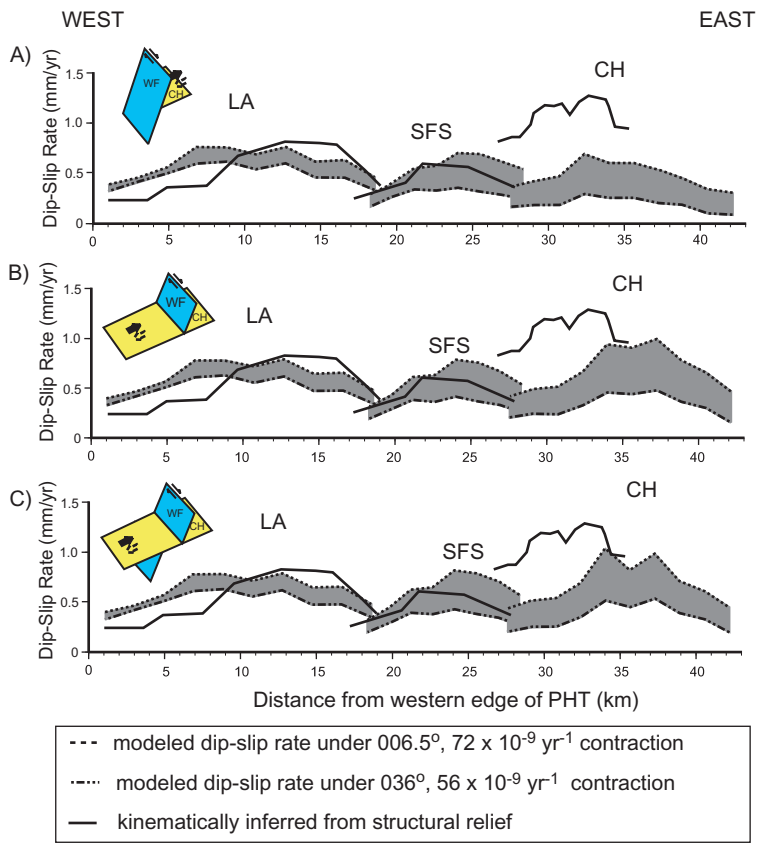


Figure 5

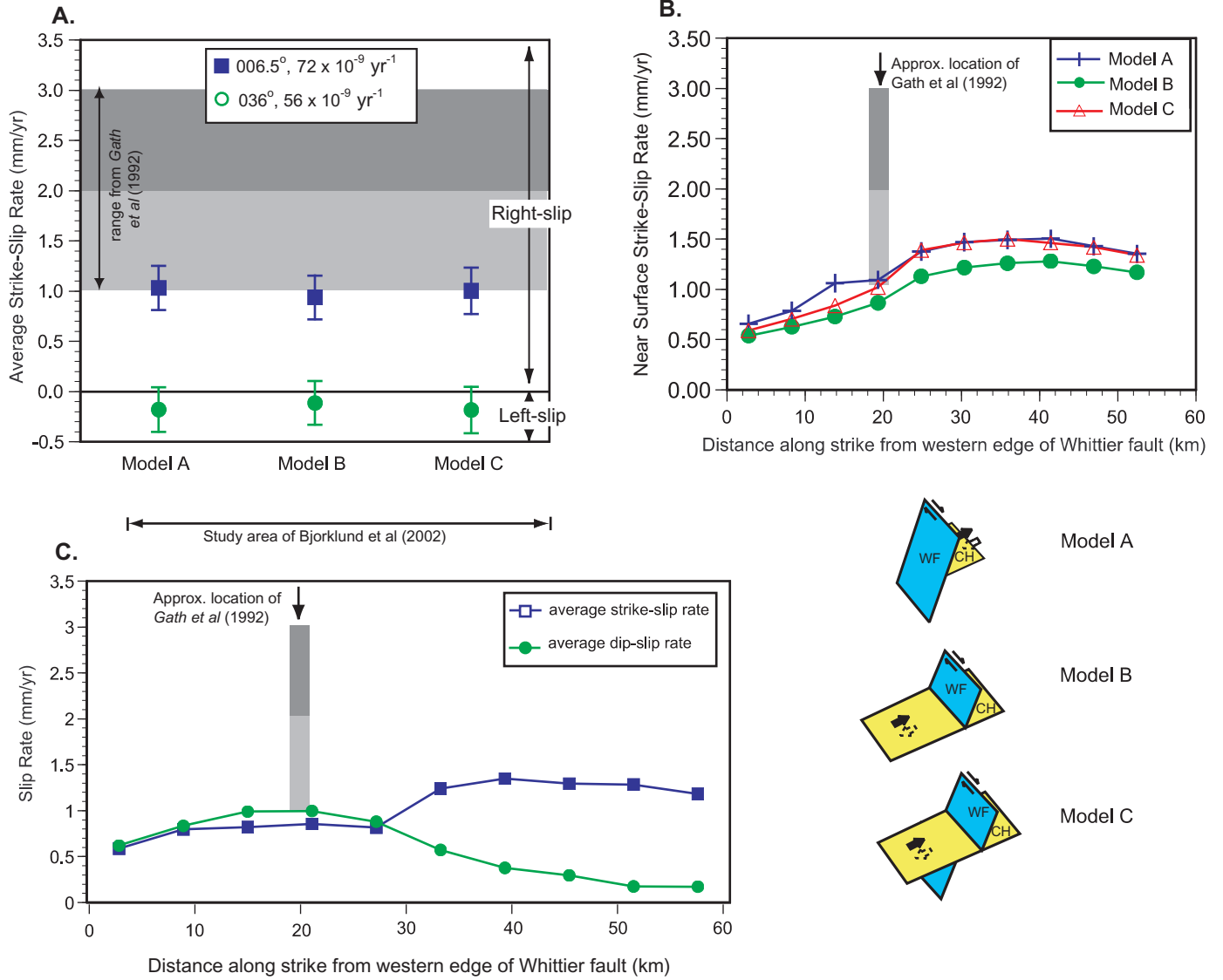


Figure 6

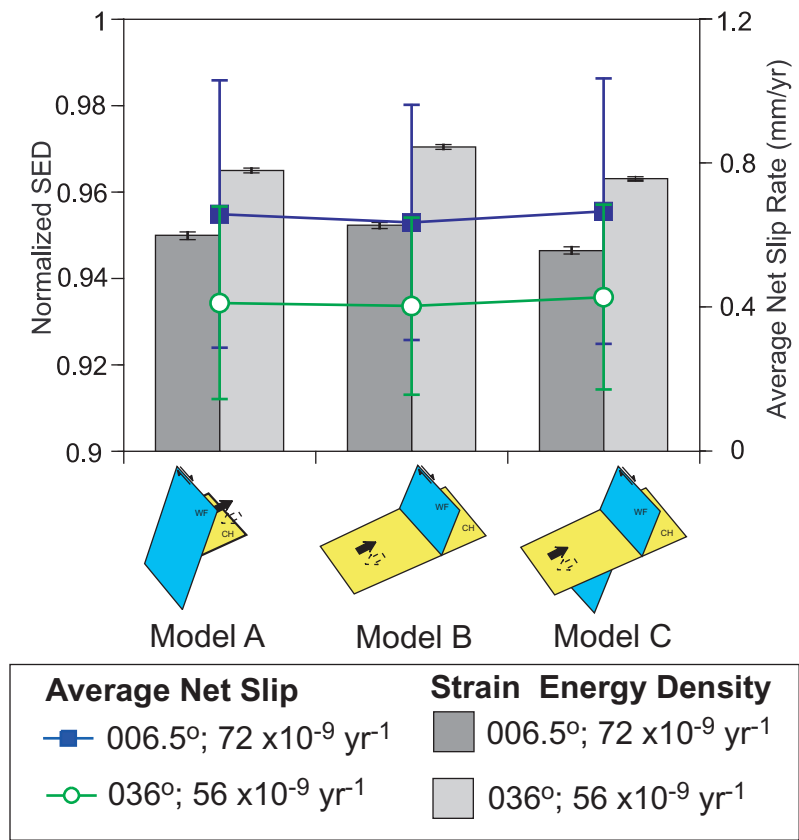


Figure 7